Next Energy 10 (2026) 100489

Contents lists available at ScienceDirect

Next Energy

journal homepage: www.sciencedirect.com/journal/next-energy

Research article

Dynamic simulation of a PEM fuel cell: Insights into efficiency, thermal, and fluid management

Theodore Azemtsop Manfo

Department of Electrical Engineering and Energy Technology, School of Technology and Innovations, University of Vaasa, Wolffintie 32, Vaasa 65200, Finland

ARTICLE INFO

Keywords:
Proton exchange membrane fuel cell
Dynamic modeling
MATLAB/Simulink
Thermal and fluid management
Hydrogen utilization
System efficiency
Renewable energy integration

ABSTRACT

Proton exchange membrane (PEM) fuel cells are emerging as critical technology for clean and efficient energy conversion, providing a path to worldwide decarbonization and renewable power generation. Their successful integration into renewable and hybrid systems necessitates a thorough understanding of the interconnected electrochemical, thermal, and fluid processes that regulate performance. However, many existing models oversimplify these dynamic interactions, resulting in an inadequate understanding of system-level behavior and control optimization. This study fills that gap by creating a dynamic MATLAB/Simulink-based model of a PEM fuel cell to investigate how integrated thermal and fluid management affect efficiency, gas usage, and operational stability under changing loads. The model includes several critical subsystems, including the membrane electrode assembly, gas flow routes, heat regulation, and purge control. Simulation findings show a peak electrical output of 95 kW with a power density of 1.116 W cm^{-2}. This highlights the need for active cooling and purging strategies in reducing hydrogen loss and preserving stack performance. The findings aid sustainable PEM fuel cell design and real-time control development.

1. Introduction

Proton exchange membrane (PEM) fuel cells are becoming popular for clean energy conversion due to their high efficiency, small size, low-temperature operation, and quick start [1,2]. PEM fuel cells are especially appealing for electric vehicle (EV) applications due to their high electrical efficiency, which is often more than double that of internal combustion engines. They also operate at low temperatures and pressures, offer high power and energy density, and produce very low noise emissions. These characteristics make PEM fuel cells crucial for achieving sustainable mobility and meeting the clean energy goals outlined in Sustainable Development Goal 7 [3].

These systems electrochemically convert hydrogen and oxygen into electricity, generating water and heat as byproducts, and have a great potential for integration with renewable energy systems [4,5].

Modeling and simulation are critical components in the design, control, and optimization of PEM fuel cell systems, particularly under dynamic and transient load situations. MATLAB/Simulink has evolved as a popular tool for creating component-based models that incorporate electrical, thermal, fluid, and control subsystems [6–8]. These models enable real-time monitoring of hydrogen consumption, current-voltage (I-V) characteristics, membrane hydration, and heat rejection, all of which are critical for assessing performance under changing load profiles [9,10].

The appropriate representation of the membrane electrode assembly (MEA) is critical in PEM fuel cell modeling because it influences electrochemical behavior and losses due to activation, ohmic resistance, and mass transport restrictions [11,12]. Recent research has highlighted the importance of combining thermal and water management subsystems with the MEA for forecasting events such as membrane dehydration, floods, and thermal runaway [13,14]. Active cooling, purge control, and humidification strategies have been proposed to improve thermal stability and membrane conductivity across a wide range of operating conditions [15,16].

This study creates a MATLAB/Simulink-based dynamic model of a PEM fuel cell system that incorporates electrochemical, thermal, and control subsystems to assess performance under transient loading conditions. The model's subsystems include hydrogen and air flow paths, MEA, humidification units, coolant loop, purge control, and real-time feedback controllers. The goal is to determine how variations in power demand and environmental circumstances influence electrochemical performance, system efficiency, and gas purity. The simulation findings are utilized to gain insights into fuel cell control techniques, energy efficiency, and hybrid system design.

2. System description and modeling approach

In a PEM fuel cell, heat is generated mainly through electrochemical reactions and resistive losses in the cell components.

E-mail address: theodore.azemtsop.manfo@uwasa.fi.

https://doi.org/10.1016/j.nxener.2025.100489
Received 4 October 2025; Received in revised form 19 November 2025; Accepted 21 November 2025

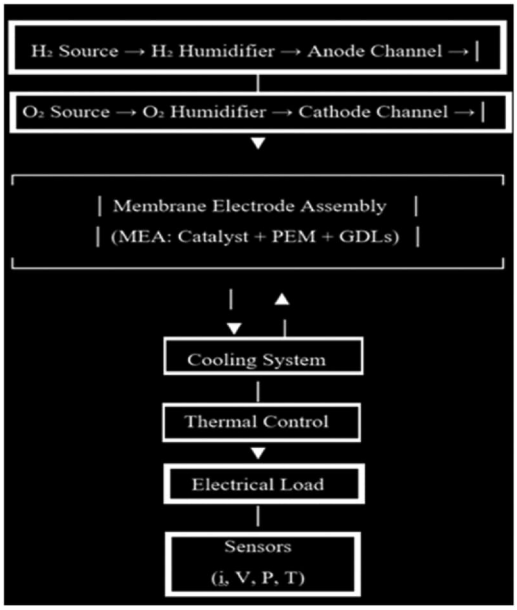

Fig. 1. Proposed schematic diagram of the optimized PEM fuel cell model. GLDs = gas diffusion layers; MEA = membrane electrode assembly; PEM = proton exchange membrane.

Hydrogen oxidation at the anode and oxygen reduction at the cathode release energy, which is partly converted into electrical power and partly lost as heat. This thermal energy arises from the irreversibility of electrochemical reactions, resistances to proton and electron transport, and gas diffusion within the flow fields. The heat generated depends on factors like current density, reactant utilization, and membrane water content. Effective thermal management is crucial to maintain temperature uniformity, prevent membrane dehydration or flooding, and ensure system durability and efficiency, especially in fuel cell EVs, where dynamic load conditions can increase heat transients [17].

2.1. Overview of system architecture

A dynamic system-level model of a PEM fuel cell was created in MATLAB/Simulink to simulate its electrochemical and thermal behavior under changing operating circumstances. The model is made up of interrelated subsystems such as the fuel cell stack, electrical input, gas supply and circulation, water management, and temperature control (Fig. 1).

The fuel cell stack model uses a semi-empirical voltage expression that accounts for the reversible Nernst potential as well as losses caused by activation, ohmic, and concentration overpotentials.

2.2. Hydrogen source

The Hydrogen Source stores and provides pressurized hydrogen (H_2) to the anode side. Hydrogen acts as fuel and is oxidized, releasing protons and electrons [18]. It is a vital fuel supply component of the PEM fuel cell system, ensuring that hydrogen is delivered cleanly, consistently, and safely for efficient and reliable power generation.

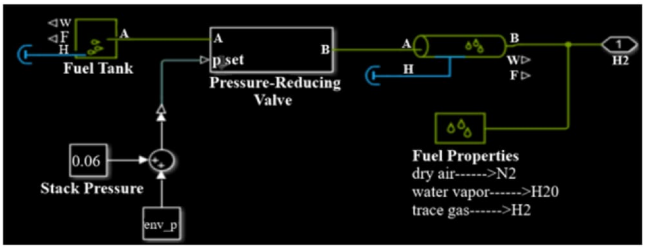

2.3. Anode humidifier

The Anode Humidifier maintains appropriate membrane hydration by managing the humidity of the hydrogen supply, improving the PEM fuel cell stack's ionic conductivity, efficiency, and lifetime. It moistens incoming H_2 to maintain membrane hydration, essential for strong proton conductivity and preventing drying [19].

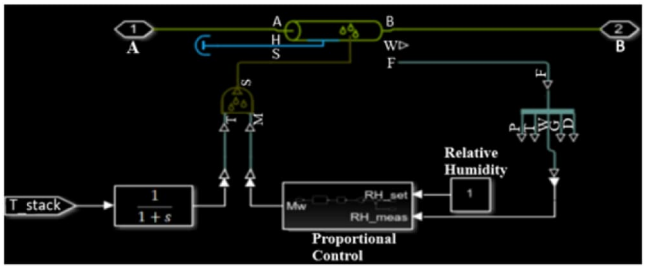

2.4. Anode flowfield

The Anode Flowfield is critical for hydrogen distribution, water and gas management, and overall electrochemical uniformity, and has a direct impact on the PEM fuel cell stack's performance, durability, and efficiency. It distributes humidified hydrogen evenly throughout the catalyst layer, facilitating effective electrochemical reactions [20].

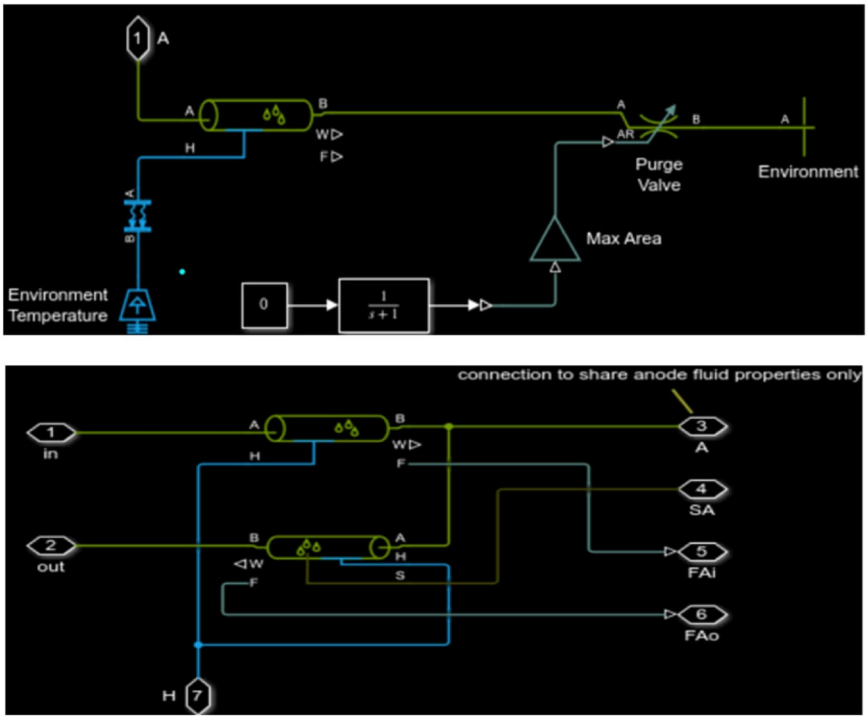

2.5. Membrane electrode assembly (MEA)

The MEA is the heart of the PEM fuel cell, where electrochemical processes occur to convert hydrogen and oxygen into electricity, water, and heat, while also assuring effective proton transport, electron flow, and water management. This includes:

- PEM: protons are conducted from the anode to the cathode.
- Catalyst layers: facilitate hydrogen oxidation (anode) and oxygen reduction (cathode) processes.
- Gas diffusion layers: maintain uniform gas distribution and water management.

Electro-osmotic drag, reverse diffusion, and humidification all affect water balance in the PEM fuel cell model. To maintain proton conductivity, the anode humidifier keeps the hydrogen input almost saturated. Electro-osmotic drag and back diffusion compete for the dynamic membrane hydration state (λ). This water content influences membrane conductivity and overall voltage losses. A feedback-controlled humidification subsystem adjusts inlet humidity to prevent membrane drying at high current densities and flooding at low loads, thereby ensuring stable ionic transport and membrane integrity. Appendix A contains the full Simscape implementation of the MEA submodel, including parameter definitions and internal calculations.

2.6. Cathode flowfield

The Cathode Flowfield is responsible for hydration, uniform oxygen distribution, and water removal on the cathode side, enabling the PEM fuel cell to operate efficiently and reliably under varying conditions. It manages oxygen supply and humidity to efficiently support the reduction reaction, just as they do on the anode.

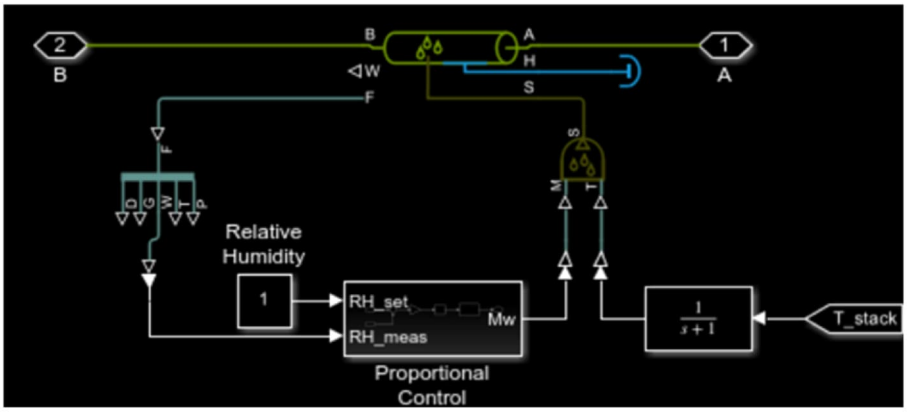

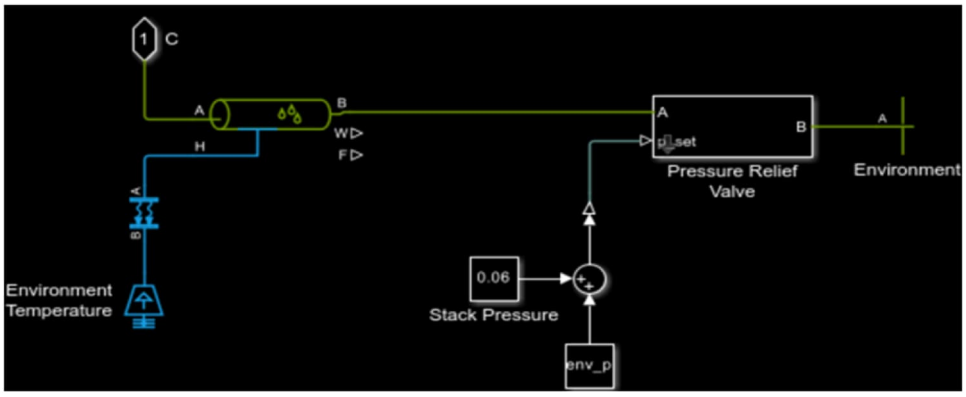

2.7. Pressure regulation valve subsystem

The pressure regulation valve subsystem guarantees that the PEM fuel cell receives gases at the proper operating pressure while protecting the system from overpressure, so contributing to both performance stability and operational safety.

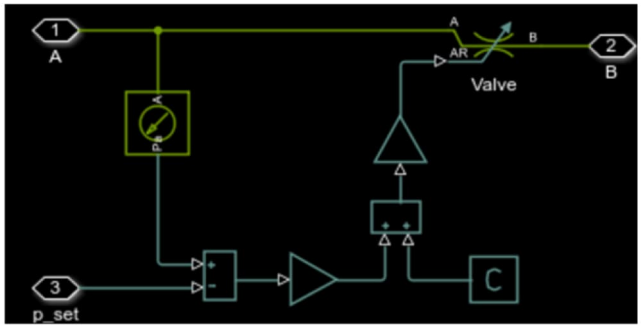

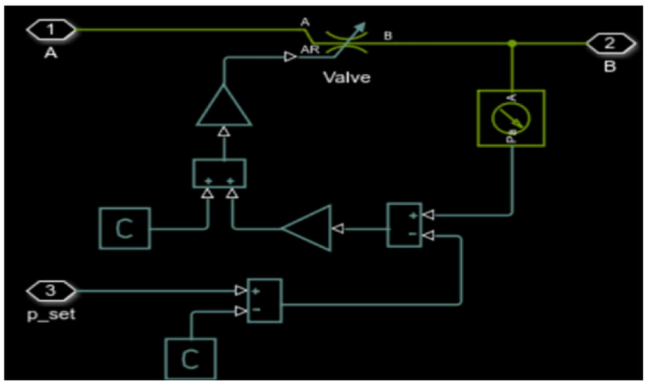

2.8. Cathode gas channels subsystem

The Cathode Gas Channels Subsystem allows for efficient oxidant supply, water management, and uniform reaction distribution, all of which are critical to the PEM fuel cell stack's efficiency, lifetime, and stability.

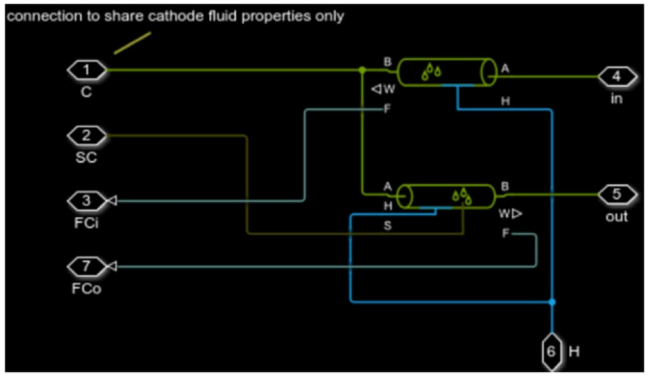

2.9. Thermal management subsystem

The thermal-management subsystem uses active coolant circulation to keep the PEM stack temperature within the specified operating range. A cascade control architecture was used, with the outer loop acting on the measured stack temperature to produce a commanded coolant mass flow rate, and the inner loop converting the mass-flow command into a pump actuator signal (pump speed or valve opening). The temperature setpoint was set at 70 °C, giving an operating margin below the model's 80 °C design limit while maintaining membrane hydration and conductivity. To mitigate the effects of quick electrical

transients on the thermal loop, the outer controller has a relatively slow integrator time constant (minutes scale), whilst the inner mass-flow loop responds faster (seconds scale), resulting in a consistent cascade response.

The PI controllers are expressed as:

$$u_T(s) = K_{p,T}\left[e_T(s) + \frac{K_{i,T}(s)}{s}e_T(s)\right] \quad (1)$$

$$u_m(s) = K_{p,m}\left[e_m(s) + \frac{K_{i,m}(s)}{s}e_m(s)\right] \quad (2)$$

where $e_T = T_{\text{set}} - T_{\text{stack}}$ is the temperature error and $e_m = \dot{m}_{\text{cmd}} - \dot{m}_{\text{meas}}$ is the mass-flow error.

Controller tuning occurred in 2 stages. First, open-loop step responses were utilized to create a reduced-order thermal model of the stack-coolant loop, which was then used to get initial gains via the Ziegler-Nichols relay method. High-fidelity Simulink models were used to optimize and improve, including limiting temperature overshoot to less than 5%, achieving settling durations compatible with the stack thermal constant ($\sim 10^2$ s), and avoiding oscillations during dynamic load phases. Anti-windup protection was implemented to prevent integrator saturation during pump restrictions and purge events. A feedforward term proportional to the instantaneous stack current was added to predict heating during large current steps, improving transient response.

The following controller parameters were utilized for reproducibility: outer PI-$K_{p,T}$=0.8, $K_{i,T}=2.0\times10^{-2}$ s^{-1}; inner PI (mass flow)- $K_{p,m}$ = 1.2, $K_{i,m}=$ 1.0×10^{-1} s^{-1}. Pump actuator limits were set per manufacturer specifications, and the integrator was clamped during saturation. Fig. 6 shows the closed-loop stack temperature and coolant mass flow for a 0→peak current step, with less than 5% overshoot and a settling period of $<$ 300 s.

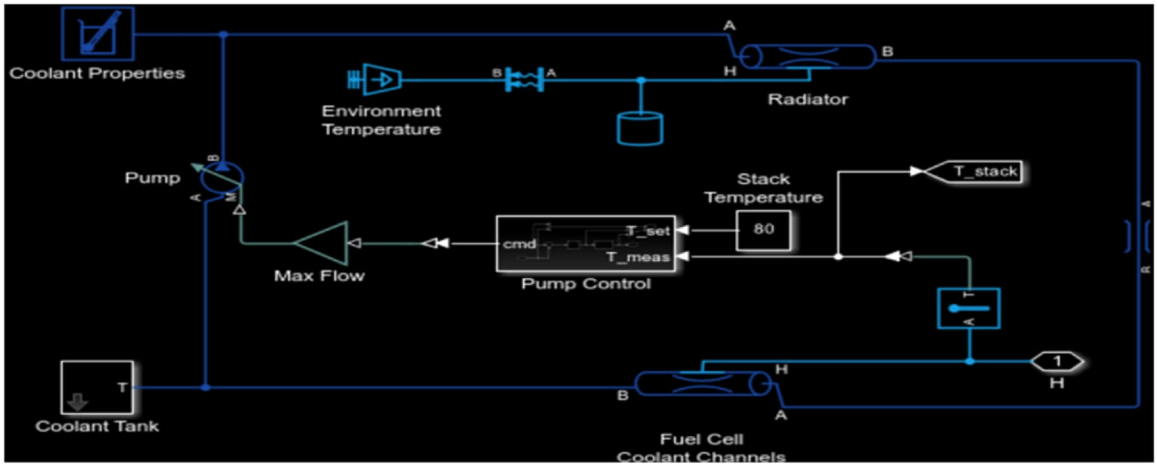

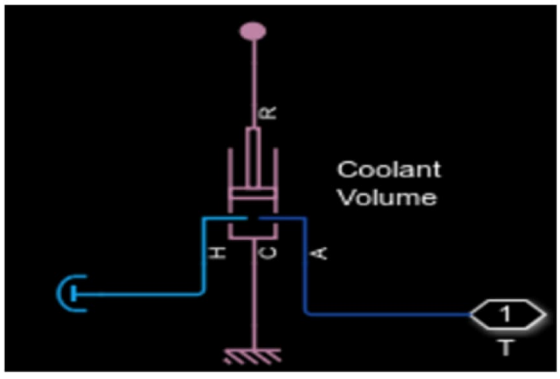

2.10. Hydrogen source subsystem

The Hydrogen Source Subsystem is the principal fuel supply unit of a PEM fuel cell system, ensuring that hydrogen is delivered safely, purely, and consistently to support efficient and long-term power generation.

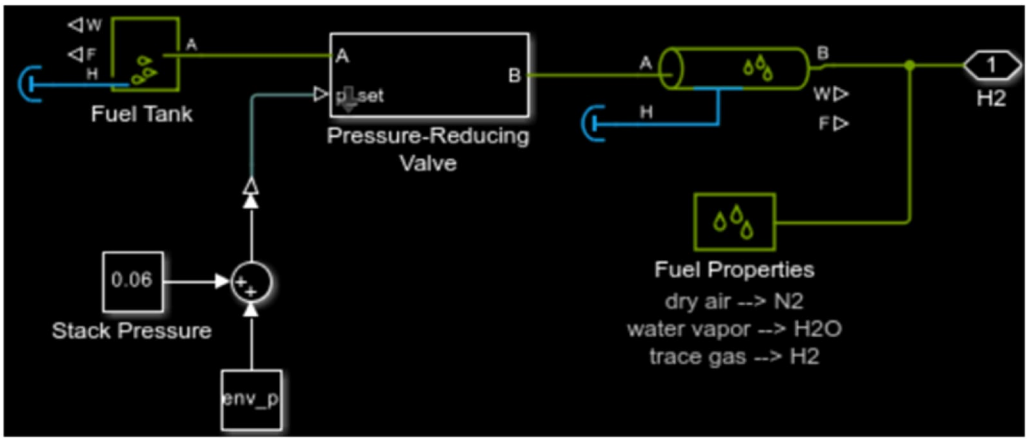

To provide comprehensive model reproducibility, Appendix B contains detailed formulations and parameter definitions for auxiliary power modeling of the compressor and coolant pump.

2.11. Oxygen source subsystem

The Oxygen Source Subsystem provides a clean, adequately pressured, and humidified oxidant feed to the cathode, allowing for stable electrochemical processes, efficient energy conversion, and longer membrane life in PEM fuel cell operation.

The compressor and coolant pump are designed as load-dependent components. Compressor electrical power is computed using the isentropic compression work required to elevate the oxidant from ambient to cathode inlet conditions, scaled by an isentropic efficiency to account for mechanical and electrical losses. Compressor mass flow is proportional to stack current via the selected stoichiometric ratio; hence, compressor power grows with load. The coolant pump's electrical power is calculated as the hydraulic power required to circulate coolant at the specified mass flow and overcome the coolant loop pressure head, divided by pump efficiency. Controller operations (cascade temperature → mass-flow command → pump actuator) affect pump speed/valve opening, resulting in immediate pump power. The 3.8 kW amount presented in Section 3.3 and Fig. 4 represents the total average auxiliary consumption for the simulated operating profile; instantaneous auxiliary power fluctuates depending on load and component efficiency.

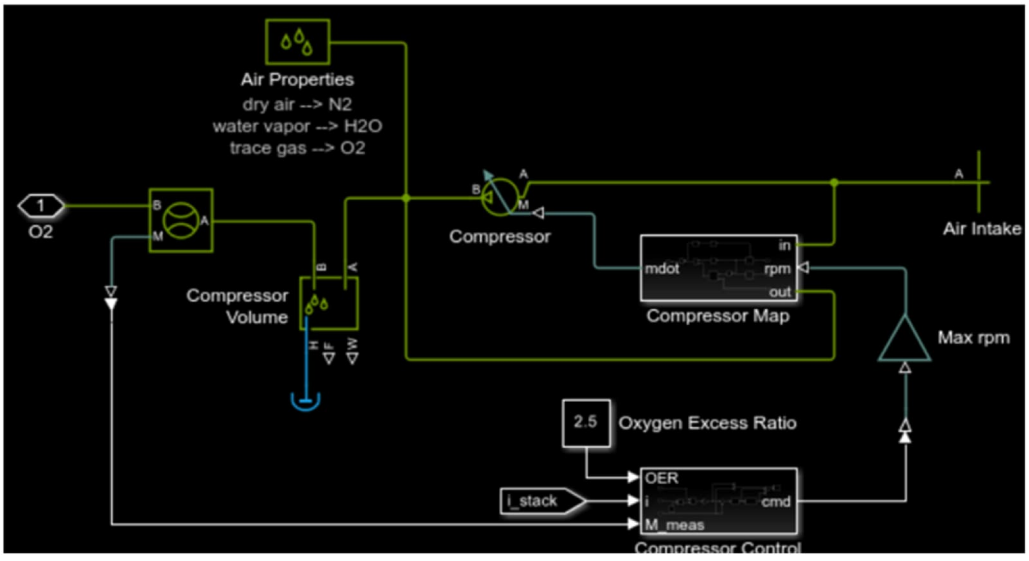

2.12. Recirculation subsystem

The Recirculation Subsystem improves hydrogen utilization, water balance, and overall system performance by recycling unreacted fuel and ensuring ideal gas flow conditions within the PEM fuel cell's anode circuit.

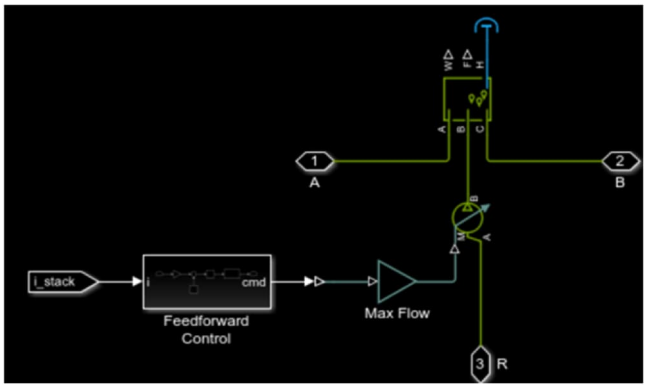

2.13. Electrical load

The Electrical Load is the final component that uses the power produced by the PEM fuel cell. It is crucial for determining the operating point, efficiency, and dynamic response of the complete fuel cell system. It could be resistive, dynamic, or coupled to a power conditioning circuit.

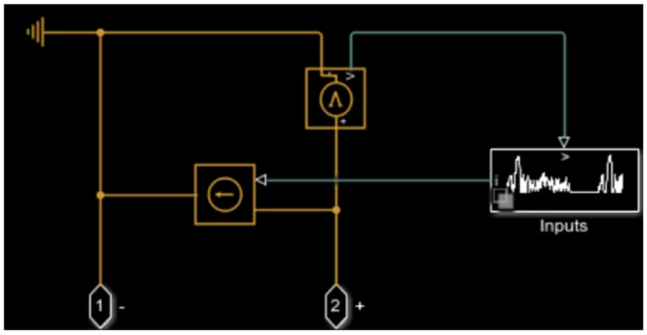

2.14. Sensors and measurement unit

The sensors and measurement unit serve as the information backbone of the PEM fuel cell system, ensuring safe, efficient, and dependable operation via accurate monitoring, feedback control, and diagnostic capabilities. It monitors important parameters such as voltage, current, power, pressure, and temperature (i, V, P, T) for system control and diagnostics.

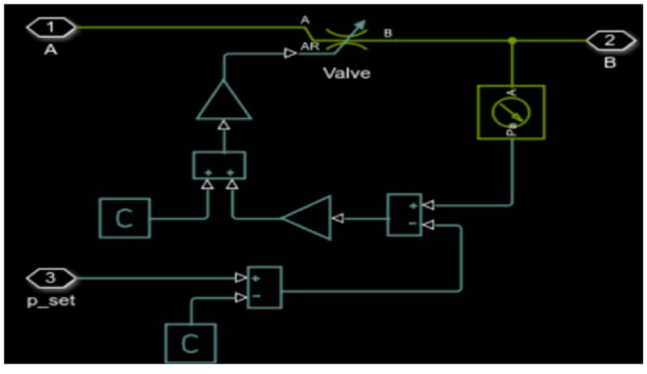

All subsystems are connected by signal lines that represent electrical, thermal, and fluid interactions. The model may work in both steady-state and dynamic load scenarios. Simulink's solver settings are optimized for stiff systems (e.g., ode15s) to ensure stability and convergence. The simulation results include stack voltage, power density, hydrogen consumption, thermal efficiency, and coolant requirements, all of which provide information on the PEM fuel cell system's performance and operational boundaries.

3. Results

3.1. Dynamic electrical and thermal response (scopes output)

Fig. 2 depicts the simulated dynamic performance of a PEM fuel cell stack, including current, voltage, power, and temperature profiles. The current response varies dramatically between 0 and 200 A, indicating varied load circumstances and exhibiting the stack's quick dynamic response capacity. The associated voltage trace shows the characteristic polarization trend, with voltage falling as current increases due to activation and ohmic losses, then quickly rebounding during low-load times. As a result, the electrical power output peaks around 100 kW at intermediate current levels, which corresponds to the stack's maximum power point. The heat generated follows a similar trend, but is much lower than the electrical output, demonstrating the model's effective conversion efficiency and stable energy balance. The stack temperature steadily rises from ambient to around 80 °C before stabilizing, showing good thermal management and consistent heat removal throughout continuous operation. Overall, the I-V-P-T characteristics show that the simulated PEM fuel cell model accurately reproduces the coupled electrochemical and thermal dynamics under transient operating conditions, making it suitable for performance evaluation and system-level integration studies in next-generation energy systems.

3.2. Steady-state polarization curves (Simscape logging)

Fig. 3 shows the I-V and current-power (I-P) curves for the PEM fuel cell block system.

The graph (in blue) depicts the I-V curve of the PEM fuel cell block system in the stack. As the current increases, the voltage drops, first due to electrode activation losses, then progressively due to ohmic resistances. Gas transport losses cause a rapid reduction in voltage near the maximum current.

The picture (in red) also illustrates the power output of the PEM fuel cell system. When the ramp scenario is selected, the power increases until it reaches its maximum output, at which point it drops due to substantial losses near the maximum current.

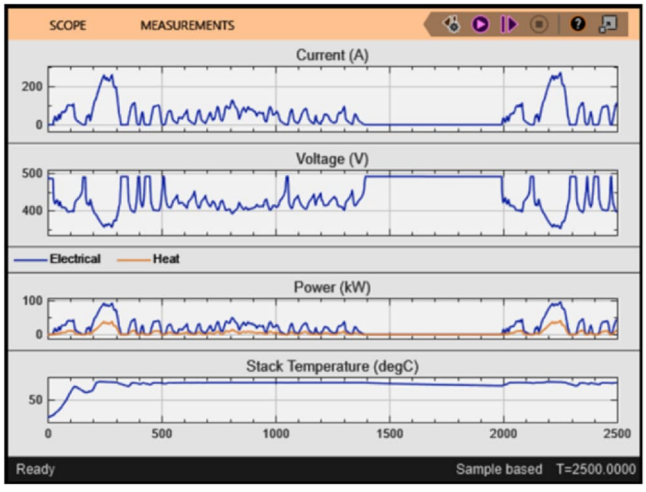

Fig. 2. Current (I), voltage (V), and power (P) characteristics from Scopes.

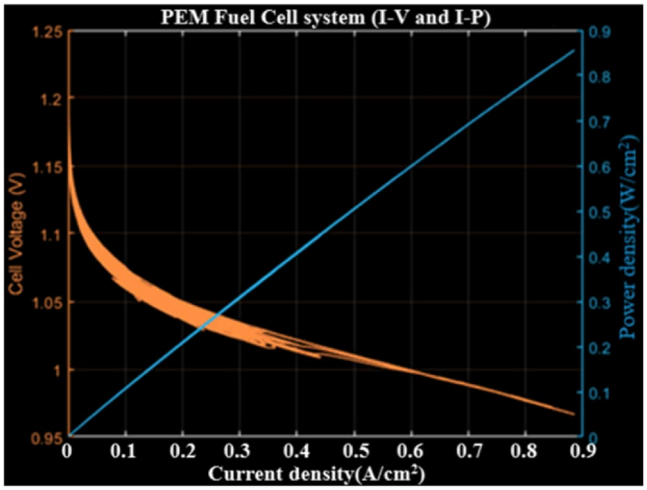

Fig. 3. I-V and I-P curves. I-P = current-power; I-V = current-voltage.

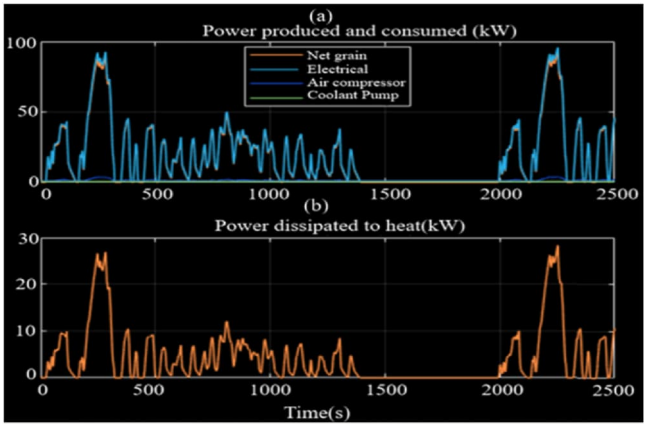

Fig. 4. (a) Power produced and consumed (kW) and (b) Power dissipated.

3.3. Power distribution and energy balance

Fig. 4 demonstrates how electrical power is distributed in the PEM fuel cell system, including input to the PEM fuel cell stack and consumption by auxiliary components such as the cathode air compressor and coolant pump. These ancillary systems are essential for maintaining steady and effective operation. As a result, the net power input to the fuel cell stack is somewhat lower than the overall electrical power output.

The model assumes that the compressor has ideal isentropic behavior; however, allowing for real-world compressor efficiency might result in a slight increase in overall power consumption. Furthermore, the image illustrates the thermal energy generated during operation, which must be dissipated by the cooling system to keep the stack within its temperature limits. The device can produce a maximum electrical power output of 95 kW. The stated ~3.8 kW auxiliary load is the average electrical consumption of compressor(s) and coolant pump for the simulated load profile. Instantaneous auxiliary power is load-dependent and computed using the isentropic compressor and pump hydraulic relations specified in the Methods.

3.4. Efficiency and reactant utilization

Fig. 5(a) depicts the fuel cell's thermal efficiency and reactant utilization fraction. The thermal efficiency of a fuel cell reflects how much energy from hydrogen fuel is converted into useful electrical work. A PEM fuel cell can theoretically achieve an efficiency of 83%. However,

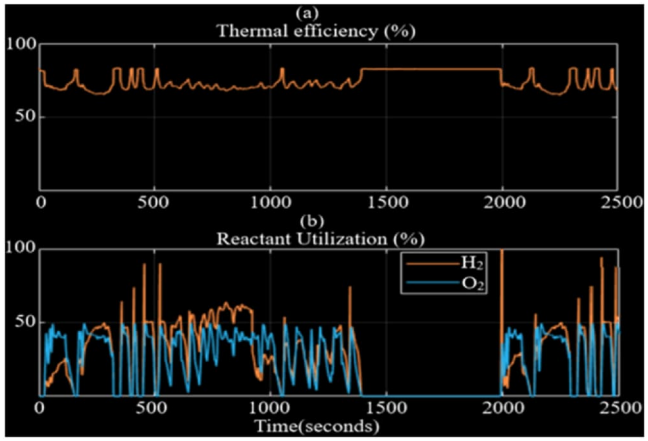

Fig. 5. (a)Variation of thermal efficiency(%) and (b) reactant utilization(%) vs. time.

internal losses reduce efficiency to about 60%. Near maximum current, efficiency has reduced to roughly 45%.

Reactant usage is the fraction of reactants (H_2 and O_2) that enter the fuel cell stack and are utilized by the fuel cell, as shown in Fig. 5(b). Higher utilization makes better use of the gases flowing through the fuel cell, but it reduces reactant concentration, lowering voltage output. Unconsumed O_2 is discharged into the environment, whereas unconsumed H_2 is recirculated back to the anode to reduce waste. Impurities are removed from H_2 at regular intervals.

3.5. Thermal regulation and coolant flow

To evaluate the model's dynamic reactivity, a step-load test was performed with the stack current increasing from 0 A to 200 A. Fig. 6 shows the transient behavior of voltage, temperature, and coolant mass-flow rate. The voltage dips by around 3% for a brief period before recovering within 1–2 s, demonstrating the stack's quick electrochemical response. The temperature gradually rises toward the 80 °C setpoint, with less than 5% overshoot, suggesting that the cascade control loop is effectively regulating thermal energy. The coolant mass-flow rate fluctuates proportionally to the heating rate, ensuring stable operation during the transient. These findings demonstrate that the developed PEM fuel cell model accurately reproduces system dynamics and performs consistently under rapid load variations.

Fig. 6(a) depicts the temperature distribution in several regions of the PEM fuel cell system. The system's cooling loop maintains the stack temperature at a maximum of 80 °C to optimize performance and prevent membrane breakdown. As part of the thermal dynamics, the recirculating hydrogen stream absorbs heat as it returns to the anode, while air compression on the cathode side contributes to the temperature rise.

Maintaining correct heat management is critical because high temperatures reduce membrane hydration and ionic conductivity, whereas low temperatures increase resistance. The proposed model controls temperature by altering the coolant pump's mass flow rate in real time. Fig. 6(b) displays the development of coolant temperature as it absorbs heat from the stack and releases it via the radiator. This process is associated with a progressive decline in hydrogen tank pressure as the gadget converts electrical input into stored hydrogen. The simulation confirms the usefulness of active cooling in regulating operational temperature and enhancing hydrogen production efficiency.

3.6. Fuel storage and gas management

Fig. 7 shows the time evolution of hydrogen storage and energy flow parameters when the PEM fuel cell system operates dynamically.

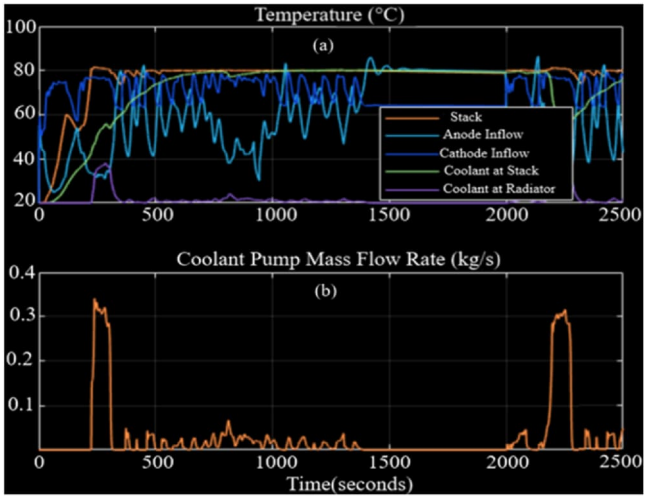

Fig. 6. (a)Variation of temperature (°C) and (b) Coolant pump mass flow rate (kg/s) with time.

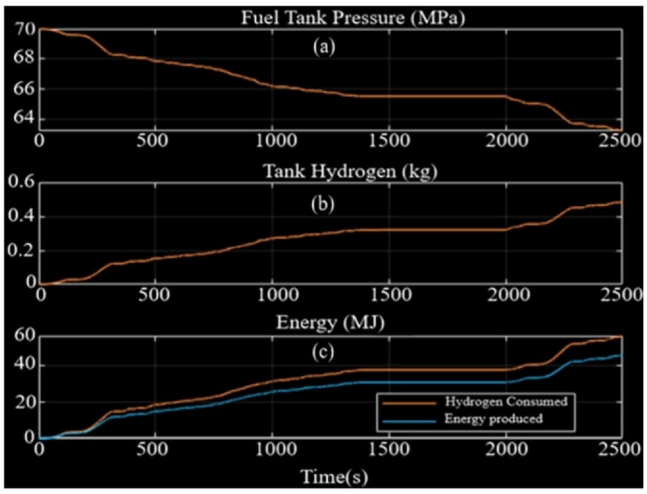

Fig. 7. Dynamic behavior of the PEM fuel cell system: (a) Fuel tank pressure, (b) Hydrogen mass in tank, and (c) Energy consumption and production vs. time. PEM = proton exchange membrane.

Fig. 7(a) shows that the fuel tank pressure gradually decreases from approximately 69 MPa to 64 MPa over a 2500-s simulation time. This slow decline is caused by the constant withdrawal of hydrogen to power the fuel cell stack. The relatively smooth pressure reduction indicates that the pressure-reducing valve is effectively controlling mass flow and consuming hydrogen at a consistent pace. The lack of significant fluctuations shows that the fuel delivery subsystem is in a stable state, with no transients or oscillations in the supply line.

Fig. 7(b) demonstrates that the hydrogen mass within the tank increases monotonically with time. This trend represents the total hydrogen input during the refueling or recirculation process, depending on the system's operational mode. The association between tank mass and pressure profile demonstrates that storage dynamics are driven by thermodynamic relationships between pressure, temperature, and mass. The trend's minor curvature could be attributed to nonlinearities in compressibility or temperature fluctuations during gas expansion and compression.

Fig. 7(c) compares hydrogen consumption to energy generated by a PEM fuel cell. The system efficiently transfers hydrogen's chemical energy into electrical energy, as evidenced by the increasing value over time. The proximity of the 2 curves throughout the experiment suggests that the fuel cell has a rather high conversion efficiency. However, a consistent discrepancy between the 2 curves suggests that conversion losses are unavoidable due to electrochemical inefficiencies, ohmic resistances, and auxiliary power usage. The total energy produced is roughly 40 MJ, as opposed to the 50 MJ of hydrogen energy required, implying an average system efficiency of around 80%, which is consistent with typical PEM fuel cell performance under dynamic settings.

Overall, Fig. 7 highlights the coupled dynamics of hydrogen storage and energy output, demonstrating that the system operates stably with predictable energy conversion behavior. The observed trends show that the simulation model is accurate in capturing transient effects in hydrogen usage, pressure dynamics, and power production efficiency.

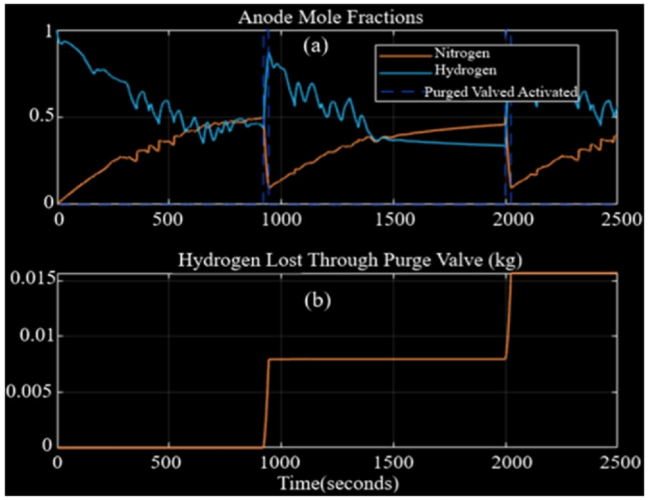

Fig. 8. (a) Anode mole fractions and (b) Hydrogen lost through purge valve (kg).

3.7. Anode gas composition and purge losses

Fig. 8 depicts the fluctuation in molar percentages of nitrogen and hydrogen within the anode compartment of the PEM fuel cell system, as seen in Fig. 8(a) and (b), respectively. Increased nitrogen concentrations relate to a decrease in hydrogen availability, which has a negative influence on electrochemical performance due to reactant stream dilution.

To manage gas composition in the anode, the system contains a purge valve with a high hydrogen content. The valve opens when the nitrogen molar percentage exceeds 50% and remains open until the concentration drops below 10%. Although this technique effectively removes excess nitrogen, it also causes unintentional hydrogen loss during purging. As a result, purge valve operation needs a well-designed control strategy that reduces hydrogen waste while maintaining system performance and gas purity. The purge thresholds (50% and 10%) were chosen based on empirical experience and proven through dynamic simulations as effective limits for preserving gas purity while minimizing hydrogen losses [21–23].

4. Discussion

The results obtained from the Simulink-based PEM fuel cell model provide valuable insight into the performance characteristics, operational limitations, and optimization opportunities of system-level hydrogen production under dynamic conditions. This is consistent with previous research emphasizing system-level modeling and management of PEM fuel cells under varying loads [24–26].

Fig. 1 illustrates the modular architecture of the system, integrating an MEA with thermal and fluidic networks. This configuration successfully captures the interaction between electrical input, water flow, and heat management, 3 critical domains in the PEM fuel cell. The

importance of these interactions has been highlighted in recent simulation and control-oriented studies[25,27,28].

Fig. 2 shows that the dynamic voltage and temperature responses confirm the realism of the PEM fuel cell model. The rapid voltage drops and recovery during load changes properly reflect activation and ohmic effects, while the steady temperature rise and stabilization near 80 °C demonstrate proper thermal management. The coupled electrical and thermal behavior shows genuine electrochemical-thermal coupling, demonstrating that the model accurately reflects the stack's transient dynamics under changing operating circumstances.

Fig. 3 shows the characteristic I-V and I-P behavior. The nonlinear shape of the I-V curve is consistent with known electrochemical losses: activation overpotentials dominate at low currents, ohmic resistance prevails in the mid-range, and mass transport limitations appear at high current densities. The I-P curve demonstrates a peak in output power, beyond which performance degrades due to increased system losses, validating the importance of operating within optimal current density ranges. These findings support the voltage behavior trends presented in [29,30], in which advanced modeling verifies comparable curve patterns and current-density effects on voltage drop and power output.

Fig. 4(a) shows the energy split between the fuel cell stack and the balance-of-plant (BoP) components. Auxiliary loads like compressors and coolant pumps consume around 3.8 kW of the 95 kW total power output, which aligns with energy consumption patterns in hybrid PEM systems [31]. Fig. 4(b) shows thermal losses of up to 28 kW, highlighting the importance of thermal control, which aligns with CFD-based research on PEM heat rejection techniques [21]. The system's total output is capped at 95 kW, with approximately 3.8 kW attributed to auxiliary consumption. Fig. 4(b) reveals substantial thermal losses (up to 28 kW), emphasizing the importance of efficient heat removal mechanisms, highlighting the importance of thermal control findings congruent with CFD-based studies on PEM heat rejection techniques [21].

Fig. 5(a) confirms that the cooling loop effectively maintains the stack temperature below the design threshold of 80 °C. Temperature regulation is essential not only to preserve MEA integrity but also to avoid dehydration or excessive membrane swelling. Preserving MEA hydration and mechanical stability in this range is critical, as evidenced by studies on membrane dehydration effects and mitigation strategies [32,33]. Fig. 5(b) shows how the coolant absorbs and transports waste heat through the radiator, while simultaneously tracking hydrogen consumption and its impact on tank pressure. This indicates how the coolant system promotes waste heat recovery while indirectly measuring reactant usage, which is consistent with advanced thermal network models [34]. The water management system successfully kept the membrane hydrated under a variety of loading conditions. The equilibrium between electro-osmotic drag and back diffusion enabled consistent water activity across the membrane, as shown by stable voltage and temperature responses. The humidifier's feedback control prevented performance degradation caused by dehydration or flooding, demonstrating the long-lasting effectiveness of the dynamic model's integrated water management method. Appendix C details the water transport methods, including electro-osmotic drag, reverse diffusion, and humidification control.

Fig. 6 (a-c) collectively depicts hydrogen storage behavior. The results suggest that system-level integration with energy storage infrastructure can be informed by real-time monitoring of tank pressure, hydrogen mass, and thermal energy content. Notably, the hydrogen mass flow aligns well with modeled Faraday efficiencies. These findings are consistent with control strategies for fuel cells and storage hybrids in renewable systems [26,35].

Fig. 7(a) reveals the accumulation of nitrogen in the anode loop and its impact on hydrogen molar concentration. As expected, an increase in nitrogen dilutes the reactant stream, reducing electrochemical performance. This behavior is well documented in gas management studies for PEM systems [21]. Fig. 7(b) shows hydrogen losses associated with purge valve operation. Although necessary to prevent nitrogen saturation, purge events result in H_2 wastage, necessitating a control strategy that balances gas purity with fuel conservation. According to a recent study, adjusting purge frequency through adaptive management can reduce hydrogen waste while preserving system efficiency [22,23].

Fig. 8 displays the change in gas composition inside the anode compartment. As illustrated in Fig. 8(a), increasing nitrogen mole percentages causes a drop in hydrogen concentration, resulting in reactant dilution and reduced electrochemical efficiency, a well-documented issue in gas crossover studies [21]. Fig. 8(b) displays a purge valve mechanism that activates when nitrogen levels exceed 50% and shuts down when nitrogen levels fall below 10%. While effective in maintaining gas purity, this method results in sporadic hydrogen losses. A recent study emphasizes the need for adaptive purging strategies to reduce fuel waste while preserving stack performance [22,23].

5. Model verification and validation

To ensure the accuracy and dependability of the Simulink-based dynamic PEM fuel cell model, a verification and validation process was carried out using both public experimental data and benchmark models from the literature. The goal was to make sure that the simulated system's behavior closely matched actual physical performance under similar operating conditions.

5.1. Steady-state verification

The simulation's polarization and power-current characteristics were compared to experimental data from [36] for a 1 kW PEM fuel cell stack operating at 60 °C, 1 atm, and stoichiometric ratios of 2 (H_2) and 3 (air). Fig. 3 indicates that the simulated cell voltage exhibits good agreement with the experimental polarization curve, with a maximum variance of less than ± 3% across the whole current density range (0–1 A cm^{-2}). This agreement demonstrates that the electrochemical, activation, and ohmic loss parameters were properly calibrated.

5.2. Dynamic performance validation

To evaluate transient behavior, the dynamic responses of stack voltage and temperature to a step load change were compared with the experimentally validated NREL dynamic PEM fuel cell model [37]. Both models had similar trends and settling times, with transient peak voltage and temperature responses ranging by less than 5%. These data demonstrate that the thermal and gas flow submodels used accurately capture the relationship between electrochemical and thermal dynamics as loads change.

5.3. Error analysis

The root mean squared error (RMSE) and percentage deviation (δ) measurements, defined as:

$$\mathrm{RMSE} = \sqrt{\frac{1}{N}\sum_{i=1}^{N}(V_{sim,i} - V_{\exp,i})^2} \tag{3}$$

$$\delta = \frac{|V_{sim} - V_{\exp}|}{V_{\exp}} \times 100\% \tag{4}$$

The computed RMSE between simulated and experimental voltages was 0.012 V, and the mean deviation was less than 3%, indicating a high level of model fidelity.

5.4. Discussion

The comparison of simulated and reference data shows high consistency for both steady-state and transient analysis. The polarization and dynamic response results closely reflect experimental trends,

supporting the electrochemical, thermal, and flow-field submodels. This alignment implies that the thermodynamic, electrochemical, and mass transport formulas used accurately represent the true behavior of the PEM fuel cell system under different operating situations.

Furthermore, the results in Fig. 7 demonstrate the model's predictive capability by depicting the couple dynamics of hydrogen storage and energy conversion. The consistent and monotonic connections observed between tank pressure, hydrogen mass, and energy production demonstrate that the system performs reliably and with predictable energy transformation characteristics. These trends demonstrate the model's capacity to capture transient impacts in hydrogen usage, pressure dynamics, and power production efficiency.

Overall, the strong agreement with actual and benchmark data demonstrates the resilience of the MATLAB/Simulink-based PEM fuel cell model. As a result, the model can be securely used in sophisticated integration studies involving hybrid energy storage systems, real-time control design, and performance optimization in dynamic operating scenarios.

6. Conclusions

This study developed a detailed Simulink-based dynamic model of a PEM fuel cell system, incorporating essential subsystems such as MEA, heat control, fluid dynamics, and gas management. The model accurately recreated fundamental behaviors such as I-V and I-P characteristics while also quantifying the effects of auxiliary loads and thermal losses during full system operation. Simulation findings show that the system can maintain optimal operating temperatures below 80 °C while balancing energy efficiency, hydrogen consumption, and gas purity. The examination of hydrogen and nitrogen molar compositions highlighted the necessity for effective purge management to reduce reactant loss. The model's dynamic reaction to load variations demonstrated the integrated control system's performance by displaying consistent voltage and current tracking with little overshoot. These findings validate the model's applicability for real-time system design, energy management, and renewable energy integration, providing a solid foundation for improving next-generation PEM fuel cell systems. Future work will center on experimentally validating the established model, particularly under dynamic and hybridized situations. Additional efforts will focus on integrating with hybrid energy storage systems (battery and hydrogen), optimizing purging and cooling control mechanisms, and implementing real-time energy management to improve system efficiency and durability.

Funding

This research did not receive any specific grant from funding agencies in the public, commercial, or not-for-profit sectors.

Data availability

Data will be made available on request.

Declaration of Competing Interest

The authors declare that they have no known competing financial interests or personal relationships that could have appeared to influence the work reported in this paper.

Appendix A. Supporting information

Supplementary data associated with this article can be found in the online version at doi:10.1016/j.nxener.2025.100489.

References

[1] M.A. Khan, S.R. Naqvi, S.A.A. Taqvi, M. Shahbaz, I. Ali, M.T. Mehran, et al., Air gasification of high-ash sewage sludge for hydrogen production: experimental, sensitivity, and predictive analysis, Int. J. Hydrog. Energy 47 (2022) 37374–37384, https://doi.org/10.1016/j.ijhydene.2021.11.192.
[3] S. Vengatesan, A. Jayakumar, K.K. Sadasivuni, FCEV vs. BEV—a short overview on identifying the key contributors to affordable & clean energy (SDG-7), Energy Strategy Rev. 53 (2024) 101380, https://doi.org/10.1016/j.esr.2024.101380.
[2] Z. Hu, S. Yuan, H. Wei, Z. Huang, H. Wei, S.H. Chan, et al., High-pressure injection or low-pressure injection for a direct-injection hydrogen engine? Int. J. Hydrog. Energy 59 (2024) 383–389, https://doi.org/10.1016/j.ijhydene.2024.02.018.
[4] M.K. Shahzad, Y. Ding, H. Zhang, Y. Dong, S.R. Jamil, M. Adnan, Performance analysis of a novel combined open absorption heat pump and FlashME seawater desalination system for flue gas heat and water recovery, Energy Convers. Manag 301 (2024) 117996, https://doi.org/10.1016/j.enconman.2023.117996.
[5] Y. Li, J. Liu, F. Liu, Y. Yang, Experimental and theoretical insights into sulfur resistance of transition-metal-doped Cu–Fe spinel during chemical-looping combustion, Int. J. Hydrog. Energy 48 (2023) 16897–16909 〈https://doi.do/10.1016/j.ijhydene.2023.01.158〉.
[6] M. Wang, J. Wang, X. Zhao, G. Qin, X. Zhang, Z. Lu, et al., $CuCo_2O_4$–NiO heterostructure catalysts for hydrogen production from ammonia borane, Int. J. Hydrog. Energy 48 (2023) 19543–19553, https://doi.org/10.1016/j.ijhydene.2023.02.068.
[7] R.K. Sharma, S. Mishra, Dynamic power management and control of a PV-PEM fuel-cell-based standalone AC/DC microgrid using hybrid energy storage, IEEE Trans. Ind. Appl. 54 (2017) 526–538, https://doi.org/10.1109/TIA.2017.2756032.
[8] F.B. Ismail, H. Al-Faiz, H. Hasini, A. Al-Bazi, H.A. Kazem, A comprehensive review of the dynamic applications of digital twin technology across diverse energy sectors, Energy Strategy Rev. 52 (2024) 101334, https://doi.org/10.1016/j.esr.2024.101334.
[9] A. Martinez, G. Iglesias, Site selection of floating offshore wind through the levelised cost of energy: a case study in Ireland, Energy Convers. Manag 266 (2022) 115802, https://doi.org/10.1016/j.enconman.2022.115802.
[10] S. Mo, L. Du, Z. Huang, J. Chen, Y. Zhou, P. Wu, L. Meng, N. Wang, L. Xing, M. Zhao, Y. Yang, Recent advances on PEM fuel cells: from key materials to membrane electrode assembly, Electrochem. Energy Rev. 6 (1) (2023) 28, https://doi.org/10.1007/s41918-023-00190-w.
[11] T. Nguyen, P. Tran, N. Doan, Advanced humidification strategies for PEM fuel cells under varying load, Energy 268 (2023) 126810, https://doi.org/10.1016/j.energy.2023.126810.
[12] Y.J. Kim, S.H. Park, Flow field design and water management in PEM fuel cells: a CFD approach, Int. J. Hydrog. Energy 50 (2025) 1235–1249, https://doi.org/10.1016/j.ijhydene.2024.10.088.
[13] S. Shahgaldi, I. Alaefour, X. Li, Impact of manufacturing processes on proton exchange membrane fuel cell performance, Appl. Energy 225 (2018) 1022–1032, https://doi.org/10.1016/j.apenergy.2018.05.086.
[14] Y. Wang, Y. Pang, H. Xu, A. Martinez, K.S. Chen, PEM fuel cell and electrolysis cell technologies and hydrogen infrastructure development – a review, Energy Environ. Sci. 15 (2022) 2288–2328, https://doi.org/10.1039/D2EE00790H.
[15] P.S.L. Chen, H. Fan, H. Enshaei, W. Zhang, W. Shi, N. Abdussamie, T. Miwa, Z. Qu, Z. Yang, A review on ports' readiness to facilitate international hydrogen trade, Int. J. Hydrog. Energy 48 (2023) 17351–17369, https://doi.org/10.1016/j.ijhydene.2023.01.220.
[16] W. Chen, X. Yan, Z. Liu, X. Zhang, C. Du, Flower-like HEA/MoS_2/MoP heterostructure based on interface engineering for efficient overall water splitting, Int. J. Hydrog. Energy 48 (2023) 29969–29981, https://doi.org/10.1016/j.ijhydene.2023.04.132.
[17] D.K. Madheswaran, A. Jayakumar, E.G. Varuvel, Recent advancement on thermal management strategies in PEM fuel cell stack: a technical assessment from the context of fuel cell electric vehicle application, Energy Sources Part A Recovery Util. Environ. Eff. 44 (2) (2022) 3100–3125, https://doi.org/10.1080/15567036.2022.2058122.
[18] S.S. Kapdi, V.K. Vijay, S.K. Rajesh, R. Prasad, Biogas scrubbing, compression and storage: perspective and prospectus in the Indian context, Renew. Energy 30 (2005) 1195–1202, https://doi.org/10.1016/j.renene.2004.09.012.
[19] Y. Wang, K.S. Chen, J. Mishler, S.C. Cho, X.C. Adroher, A review of polymer electrolyte membrane fuel cells: technology, applications, and needs on fundamental research, Appl. Energy 88 (2011) 981–1007, https://doi.org/10.1016/j.apenergy.2010.09.030.
[20] T.T. Do, N. Devi, A. Arpornwichanop, Y.S. Chen, Study on the effect of cathode purge strategy on oxygen utilization of a proton exchange membrane fuel cell using oxygen, Int. J. Hydrog. Energy 141 (2024) 487–498, https://doi.org/10.1016/j.ijhydene.2024.10.088.
[21] B.H. Lim, E.H. Majlan, W.R.W. Daud, T. Husaini, M.I. Rosli, Effects of flow field design on water management and reactant distribution in PEMFC: a review, Ionics 22 (3) (2016) 301–316, https://doi.org/10.1007/s11581-016-1644-y.
[22] L. Yang, N.N. Nik-Ghazali, M.A. Ali, W.T. Chong, Z. Yang, H. Liu, A review on thermal management in proton exchange membrane fuel cells: temperature distribution and control, Renew. Sustain. Energy Rev. 187 (2023) 113737, https://doi.org/10.1016/j.rser.2023.113737.
[23] L. Xu, Z. Hu, C. Fang, L. Xu, J. Li, M. Ouyang, A reduced-dimension dynamic model of a proton-exchange membrane fuel cell, Int. J. Energy Res. 45 (12) (2021) 18002–18017, https://doi.org/10.1002/er.6945.
[24] A. Gulraiz, A.J. Al Bastaki, K. Magamal, M. Subhi, A. Hammad, S.H. Zaidi, H.M. Khalid, A. Ismail, G.A. Hussain, Z. Said, Energy advancements and integration strategies in hydrogen and battery storage for renewable energy systems, iScience 28 (3) (2025) 111945, https://doi.org/10.1016/j.isci.2025.111945.

[25] H.W. Wu, A review of recent development: Transport and performance modeling of PEM fuel cells, Appl. Energy 165 (2016) 81–106, https://doi.org/10.1016/j.apenergy.2015.12.075.
[26] A.N. Mancino, C. Menale, F. Vellucci, M. Pasquali, R. Bubbico, PEM fuel cell applications in road transport, Energies 16 (17) (2023) 6129, https://doi.org/10.3390/en16176129.
[27] A.L. Lazar, S.C. Konradt, H. Rottengruber, Open-source dynamic Matlab/Simulink 1D proton exchange membrane fuel cell model, Energies 12 (18) (2019) 3478, https://doi.org/10.3390/en12183478.
[28] V. Rahate, P.S. Agrawal, M.M.U.D. Malik, P.B. Thakare, S. Chandra, B. Singh, Digital twins in renewable energy systems: Enhancing efficiency, projecting sustainability, Leveraging AI for Innovative Sustainable Energy: Solar, Wind and Green Hydrogen, IGI Global, 2025, pp. 123–138, https://doi.org/10.4018/979-8-3373-0045-0.ch009.
[29] Q. Wu, Z. Dong, X. Zhang, C. Zhang, A. Iqbal, J. Chen, Towards more efficient PEM fuel cells through advanced thermal management: From mechanisms to applications, Sustainability 17 (3) (2025) 943, https://doi.org/10.3390/su17030943.
[30] A.U. Yakubu, J. Zhao, Q. Jiang, X. Ye, J. Liu, Q. Yu, S. Xiong, A comprehensive review of primary cooling techniques and thermal management strategies for polymer electrolyte membrane fuel cells (PEMFC), Heliyon 10 (19) (2024) e38556, https://doi.org/10.1016/j.heliyon.2024.e38556.
[31] C. Bonnet, S. Raël, M. Hinaje, S. Guichard, T. Habermacher, J. Vernier, X. François, M.C. Péra, F. Lapicque, Direct fuel cell–supercapacitor hybrid power source for personal suburban transport, AIMS Energy 9 (6) (2021) 1274–1298, https://doi.org/10.3934/energy.2021059.
[32] Y. Huang, X. Xiao, H. Kang, J. Lv, R. Zeng, J. Shen, Thermal management of polymer electrolyte membrane fuel cells: a critical review of heat transfer mechanisms, cooling approaches, and advanced cooling techniques analysis, Energy Convers. Manag 254 (2022) 115221, https://doi.org/10.1016/j.enconman.2022.115221.
[33] W. Wang, N. Li, J. Zhang, C. Zhang, L. Zhang, Thermal management analysis of proton exchange membrane fuel cell filled with phase-change material in cooling channel, Int. J. Energy Res. 2023 (2023) 9077046, https://doi.org/10.1155/2023/9077046.
[34] B. Fang, J. Luo, P.N. Njoki, R. Loukrakpam, B. Wanjala, J. Hong, J. Yin, X. Hu, J. Last, C.J. Zhong, Nano-engineered PtVFe catalysts in proton exchange membrane fuel cells: electrocatalytic performance, Electrochim. Acta 55 (27) (2010) 8230–8236, https://doi.org/10.1016/j.electacta.2010.02.048.
[35] H.W. Wu, A review of recent development: transport and performance modeling of PEM fuel cells, Appl. Energy 165 (2016) 81–106, https://doi.org/10.1016/j.apenergy.2015.12.075.
[36] Z. Guo, E. Grano, F. Mazzeo, H. de Carvalho Pinheiro, M. Carello, Calibration and validation of a PEM fuel cell hybrid powertrain model for energy management system design, Designs 9 (4) (2025) 94, https://doi.org/10.3390/designs9040094.
[37] R. Gass, Z. Li, R. Outbib, S. Jemei, D. Hissel, AlphaPEM: an open-source dynamic 1D physics-based PEM fuel cell model for embedded applications, SoftwareX 29 (2025) 102002, https://doi.org/10.1016/j.softx.2024.102002.